ADVANCES IN ATMOSPHERIC SCIENCES, VOL. 20, NO. 4, 2003, PP. 631–637

A Laboratory Modeling of the Velocity Field in the Convective Boundary Layer with the Particle Image Velocimetry Technique

LI Pingyang*[1,2] (李萍阳), JIANG Weimei[1] (蒋维楣), SUN Jianning[1] (孙鉴泞), and YUAN Renmin[3] (袁仁民)

[1] *Department of Atmospheric Sciences, Nanjing University, Nanjing* 210093

[2] *National Meteorological Center of China, Beijing* 100081

[3] *Department of Earth and Space Sciences, University of Science and Technology of China, Hefei* 230026

(Received June 20, 2002; revised May 19, 2003)

ABSTRACT

Based on the research of the convective boundary layer (CBL) temperature field in a convective tank, this paper studies the characteristics of the CBL velocity field in the convective tank. Aluminium powder (400 orders) is used as a tracer particle in the application of the particle image velocimetry (PIV) technique. The experiment demonstrates: the velocity distribution in the mixed layer clearly possesses the characteristics of CBL thermals; the velocity distribution in the top zone of the mixed layer shows entrainment layer characteristics; the vertical distribution of turbulent characteristic variables is reasonable, which is similar to field observations and other tank results; the error analysis demonstrates the validity of aluminium powder, which implies the reliability of the results.

Key words: velocity field, convective boundary layer (CBL), convective water tank, PIV technique

1. Introduction

Indoor simulation has been an important means of researching the atmosphere boundary layer, which is able to be repeated, controlled. Willis and Deardorff (1974) researched the convective boundary layer (CBL) with a convective tank in the 1970s and 1980s, Lu and Arya (1997a, b) simulated city heat island circulation using the same tank; Yuan (2000), Sun et al. (2000), and Miao et al. (2000) measured and analyzed the temperature field in the convective tank of the Anhui Institute of Optics and Fine Mechanics, Chinese Academy of Sciences, which was the first time this was done in China, and it indicated the validity of using water tank to simulate CBL.

This paper attempts to measure and analyze the characteristics of the CBL velocity field on the research of the CBL temperature field in a convective tank, and to demonstrate the validity of indoor simulation and the PIV technique.

2. Experimental setup and similarity analysis

2.1 *Convective tank and measurement method*

This experiment simulates the CBL with a capping inversion layer. Under such conditions, we use the Particle Image Velocimetry (PIV) technique to measure the turbulent velocity of the CBL. Figure 1 shows a sketch of the experimental setup. The laser beam changes to a sheet ray by going through the concave mirror, the tracer particles in the sheet ray are illuminated to display their two dimensional trajectory, and then velocities are calculated.

The following steps are performed during each experiment: (i) the tank is filled up to 20 cm with ambient temperature water (approximately 20°C); (ii) a second layer, of 15 cm depth of hot water (with increasing temperature) is stratified above the first one to generate a thermally stable zone that simulates the capping inversion of the atmosphere; (iii) aluminium powder (400 orders) is sprinkled over the tank uniformly; (iv) after waiting 3–5 minutes for any disturbances introduced during filling to damp out, the bottom of the tank is heated, (v) about 5 min after heat is applied to the lower surface, turbulent convection is completely developed and data acquisition starts. The images collected by the Charge-Coupled Device (CCD) system are saved in the computer. Every 2–3 minutes we measure temperature profiles to calculate

*E-mail: lipy@rays.cma.gov.cn

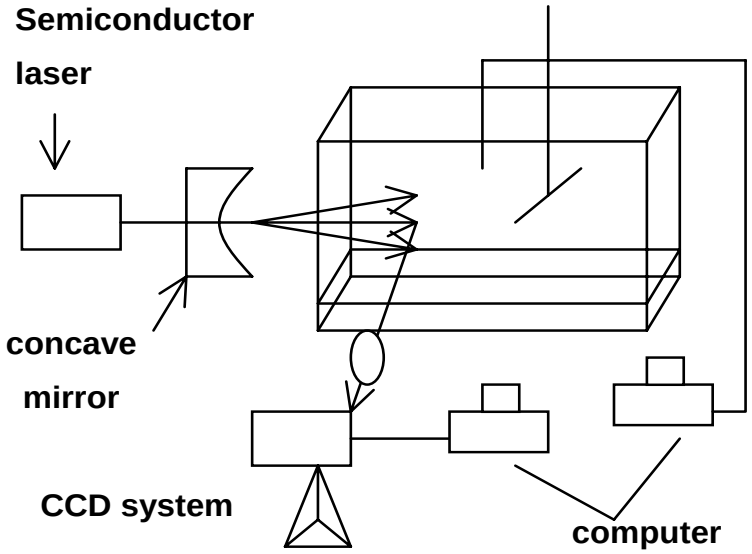

Fig. 1. Sketch of experiment setup.

the mixed layer height and the inversion layer intensity. To measure the profiles, the sensor is moved up and down, which is driven by an electromotor. The CCD visual field is near the light source in the tank, while profile measurements are performed near on the other side to reduce disturbances, as shown in Fig. 1.

2.2 *Similarity analysis*

This paper aims to study CBL above a flat underlying surface, so the convection similarity assumption is foremost (Jiang et al., 1991), namely Reynolds number (Re) similarity and Rayleigh number (Ra) similarity. The Reynolds number attainable in the tank is 10^2–10^4, while our Re based upon $Re = W_* Z_i/v$ is 2800–3900, corresponding to Willis' experiments; The Reyleigh number attainable in the tank is 10^8–10^{14}, while our Ra based upon $Ra = g\alpha Q_0 Z_i^4/vk^2$ is 10^{12}, with the same order as Willis and Deardorff's (1974). Furthermore, the characteristic value of W_* in this paper is 1 cm s^{-1}, which is the same as Willis' experiment. Thus, the flow in the mixed layer can well be considered turbulent, that is, the similarity hypothesis is valid.

3. PIV technique and velocity analysis method

3.1 *PIV technique*

The PIV (Particle Image Velocimetry) technique is a kind of image analysis technique essentially, which was developed in the past decade and has many virtues (Host-Madsen and McCluskey, 1994; Coupland et al., 1987; Lauterborn and Vogel, 1984; Willert and Gharib, 1991). Because the modeling is 3-dimensional, non-stationary, and the scale of the streamline field is wide, two conditions should be satisfied, namely, (i) the laser energy needs to be huge, and the visual field illuminated by the sheet light source should be wide; (ii) the scattering and tracing of tracers in the flow need to be good.

The CCD camera system exposes the location of particles, so we can confirm the displacement between particles by computing two records' similarity or relation. Concretely, the images are divided into some areas, the mean velocity of particles is to be computed, and then we analyze conjoint areas until we cover the entire record. The size of the area should be chosen suitably: on the one hand, enough particles should be included, for their light scattering is strong, thereby we can analyze further; on the other hand, the size should be small to ensure that the velocity in the flow cross section will not change evidently. The typical number of particles should be analyzed on the basis of fact.

3.2 *Velocity calculation method*

First, the location of the same particle in adjoining 2(or 3) pictures should be confirmed, then the particle velocity $\overline{V}$ can be calculated by formula (1).

$$\overline{V} = \frac{\Delta \overline{X}}{\Delta T} S. \tag{1}$$

Here, $\Delta \overline{X}$ is the displacement of the particle in ΔT (time interval between the conjoining 2 or 3 pictures) is, S is the ratio of picture length and actual length.

To estimate the velocity trajectory well and truly, in this paper, we use 3 conjoint pictures to confirm the velocity field, as shown in Fig. 2, where the markers

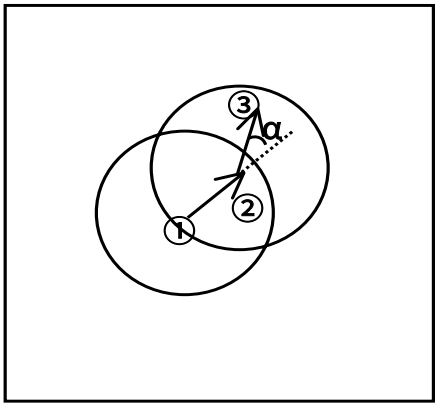

Fig. 2. Sketch map of velocity calculation method.

①, ②, and ③ denote respectively the location of the particle at t_1, t_2, and t_3. To see the idea more clearly, the velocity trajectory in the 3 pictures is described in one picture. We insure that both the distance between ① and ② and the distance between ② and ③ exceed 5 pixels, and the angle α does not exceed 1 radian; only when these three conditions are satisfied at the same time, can the three dots be the confirmed trajectory of the same particle. Such a criterion is experiential in a way, which should be adjusted in the process of analyzing data, accordingly as the velocity is in the direction of the trajectory tangent. The velocity is calculated by ① and ③, ΔT is 0.08 seconds, d is the width of the CCD visual field, S is $d/400$, namely, the actual size of the unit pixel, so the actual displacement of the particle is the product of pixel distance and the actual size of the unit pixel, and the horizontal velocity u and vertical velocity w are shown in formulae (2) and (3).

$$u = \frac{d\,(x_3 - x_1)}{400} \cdot \frac{1}{0.08}\,, \tag{2}$$

$$w = \frac{d\,(y_3 - y_1)}{400} \cdot \frac{1}{0.08}\,. \tag{3}$$

4. Velocity characteristic analysis

The visual field dimensions are 9.6 cm×9.6 cm, the vertical range of which in the tank is 14.3–23.9 cm, i.e., the bottom boundary of the pictures is at 14.3 cm, while the top boundary is at 23.9 cm. To know the relative height of tracers, the mixed layer height Z_i should be determined. In this paper, the heat flux profile method is adopted to calculate Z_i, while the heat flux profile can be obtained by measurement, particulars of which can be seen in Stull (1991) and Kaimal et al. (1976).

The velocity vectors are shown in Fig. 3a, where the mixed layer height Z_i is 17.3 cm and the particles mostly lie above the top of the mixed layer and entrainment layer. Ascending motion and the descending motion of the particles can be seen obviously, and the ascending velocity is bigger than the descending velocity, which corresponds to the field observation. Since the CCD field of view is limited, we cannot measure the ascending and descending motion in the whole tank, so we cannot be sure of the area ratio of ascending and descending velocity. During free-convection, buoyant thermals from the surface layer gain momentum as they rise through the mixed layer. Upon reaching the warmer free atmosphere they find themselves negatively buoyant, but overshoot a short distance because of their momentum. This overshooting is called penetrative convection (Deardorff, 1969). This phenomena can be observed clearly on the right of Fig. 3a (in Fig. 3a and in the following figures, to make the trend of velocity vectors more clear, we draw the main trend with a solid line; the broken line denotes the height of Z_i).

Z_i in Fig. 3b is 19.3 cm. The time interval between Fig. 3b and Fig. 3a is only 77 seconds, but the structure of the velocity field changes radically: the former descending area changes to an ascending area, while the former ascending areas in the middle and right change to a descending area. Since we cannot screen the trajectory of particles continuously, the life cycle of the eddy cannot be confirmed quantitatively, but from mere observation we can obtain that the structure will change much in one minute at least. As described by Fig. 3b, the left particles ascend into the entrainment layer, while the middle and right particles descend from the entrainment layer to the mixed layer; this process is entrainment, which corresponds to the analysis of the temperature field.

Figure 3c continues the structure of Fig. 3b; the Z_i is also close to Fig. 3b, and the whole eddy is prevenient development. As shown in Fig. 3d and Fig. 3e, the particles mostly ascend, and they begin to converge and diverge in the top of the mixed layer; the scale of the thermal is very large. The particles in Fig. 3f lie in an intensive ascending motion area, velocities are big and even, and the mixed layer height has exceeded the boundary of the lens. We can presume that the observation lies in the ascending area of a large eddy, and the scale of the eddy is likely to be on the order of Z_i. The turbulence has developed fully, and the CBL has developed very maturely.

5. Non-dimensional velocity fluctuations

5.1 *Non-dimensional horizontal velocity variance*

The non-dimensional horizontal velocity variance is plotted in Fig. 4a. As shown in the figure, there

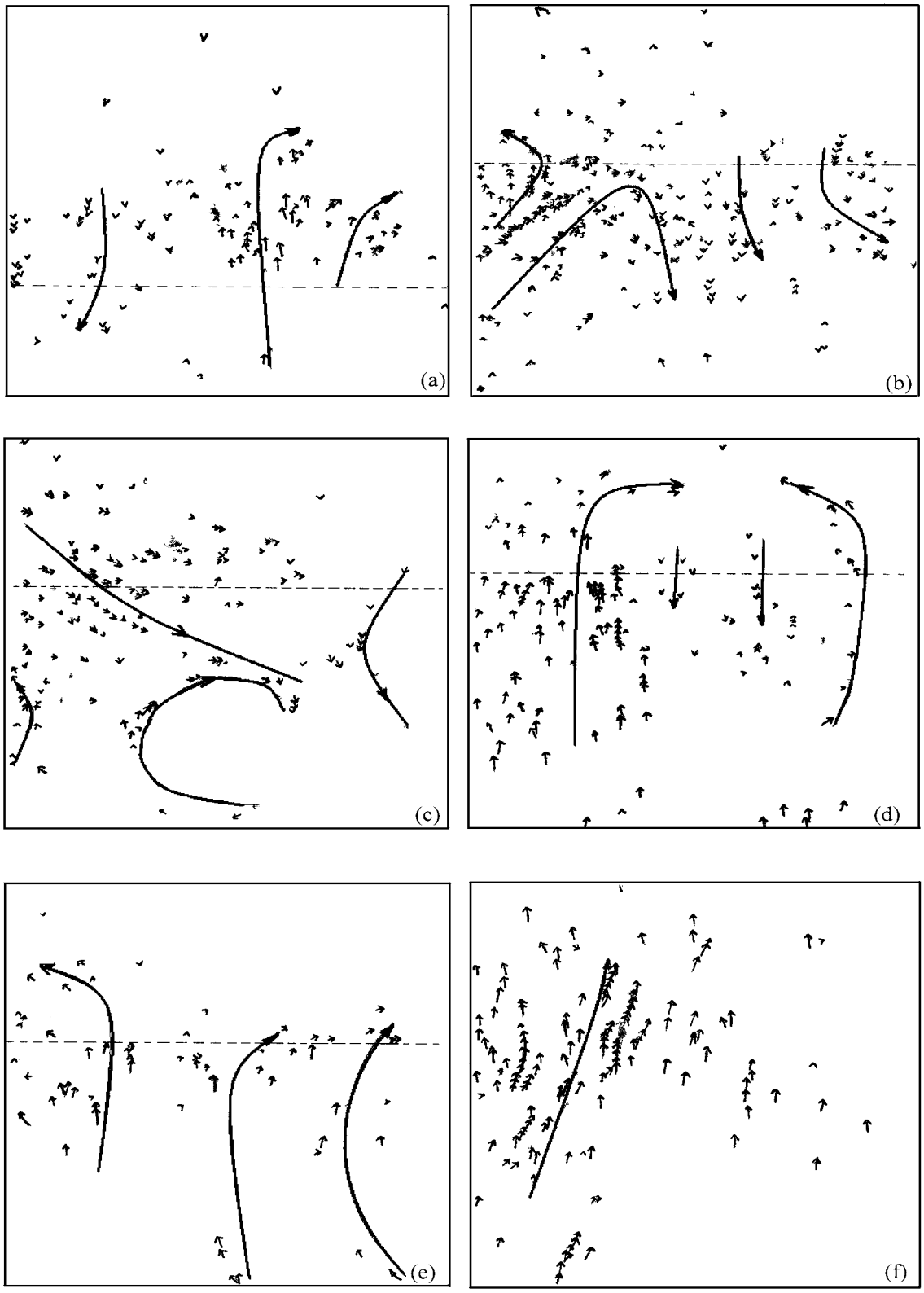

Fig. 3. Particles velocity vectorgraph (a) at 10:58, (b) at 10:59, (c) at 11:00, (d) at 11:02, (e) at 11:03, (f) at 11:09.

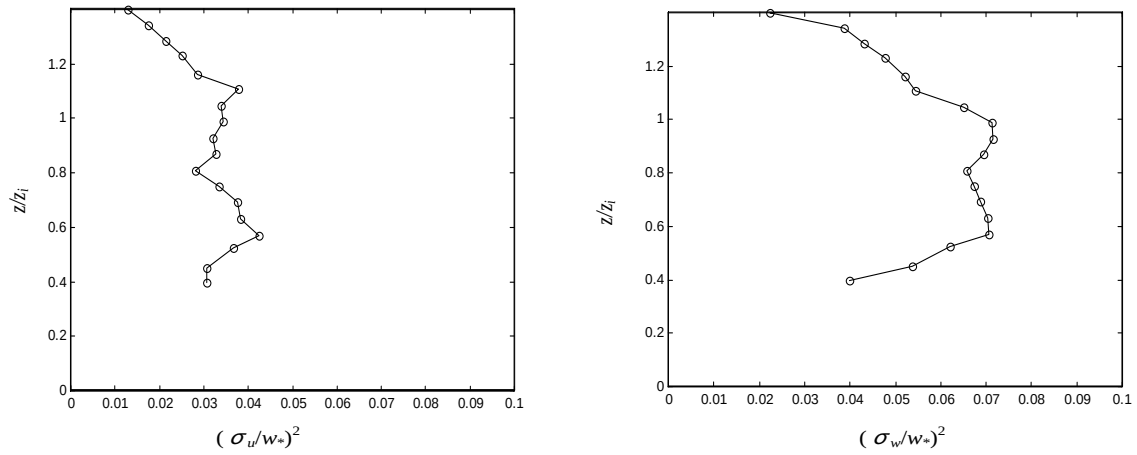

Fig. 4. Nondimensional standard deviations of velocity vs Z/Z_i: (a) horizontal velocity and (b) vertical velocity.

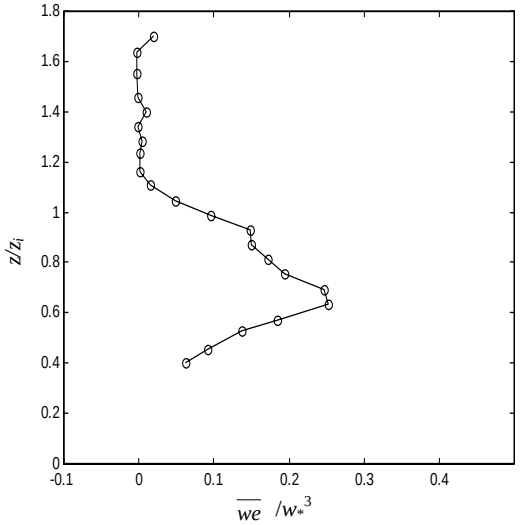

Fig. 5. Vertical profile of dimensional vertical kinetic energy flux.

is no value below Z/Z_i=0.4. This is because the laser is a sheet light source and the light intensity is correspondingly weak, so the trajectory of particles in the bottom volume of the tank cannot be obtained. The non-dimensional horizontal velocity variance increases slightly from Z/Z_i=0.45 to Z/Z_i=0.57; it approaches to some constants or changes a little in the middle and upper mixed layer, while the variance decreases with height above Z/Z_i=1.1. This trend corresponds to Willis and Deardorff's (1974) results on the whole, but the value in this paper is smaller. This discrepancy might be due to the limited CCD visual field.

5.2 *Non-dimensional vertical velocity variance*

As shown in Fig. 4b, the non-dimensional vertical velocity variance increases from a small value near the lower boundary to a maximum near the middle of the mixed layer (Z/Z_i=0.57). Above the mid-level the variance decreases with height to a small value. The trend is slightly discrepant with Willis and Deardorff's (1974) results but agrees with Lu and Arya (1997b) data very much.

5.3 *Non-dimensional kinetic energy flux*

Height is plotted against the non-dimensional kinetic energy flux, a triple correlation term, in Fig. 5. For the horizontally homogeneous case of the laboratory model, we take $\overline{we} = w\overline{(2u^2 + w^2)}/2$. It can be seen from the figure that $\overline{we}/w_*^3$ increases with height to a maximum at Z/Z_i=0.63; then it decreases with height and remains constant (zero) above the top of the mixed layer. The results agree with Willis and Deardorff (1974) very much although they are systematically larger in value, but they are close to the aircraft observations.

6. Error analysis

6.1 *The temperature error*

The accidental error of temperature measurement primarily comes from environment interference, circuit noise, and the sampling system A/D conversion. For this system, accidental error is 0.005 Volts or so. The systematic error is mainly thermal hydrometer error. The time constant of this system's fluctuating sensor is 0.1, while the time constant of the profile sensor is about 0.3. So the system of temperature measurement completely satisfies the demand of indoor simulation.

6.2 *The velocity error*

(1) Accidental error $\Delta \boldsymbol{X}$

The velocity relative error can be calculated by the error of $\Delta \boldsymbol{X}, \Delta T$ and S ($\delta_{\Delta \boldsymbol{X}}, \delta_{\Delta T}, \delta_S$). With simple differential calculation, we can get:

$$\frac{\delta_{\boldsymbol{V}}}{\boldsymbol{V}} = \frac{\delta_{\Delta \boldsymbol{X}}}{\Delta \boldsymbol{X}} + \frac{\delta_S}{S} - \frac{\delta_{\Delta T}}{\Delta T}, \tag{4}$$

where $\delta_{\boldsymbol{V}}$ is indirect error. In this paper, the error of $\Delta \boldsymbol{X}$ is far greater than that of ΔT and S, so we can consider that the error only arises from $\Delta \boldsymbol{X}$, i.e:

$$\frac{\delta_{\boldsymbol{V}}}{\boldsymbol{V}} = \frac{\delta_{\Delta \boldsymbol{X}}}{\Delta \boldsymbol{X}}. \tag{5}$$

The resolution of pixels is low when screening with a single CCD, and measurement precision will suffer certain restrictions from the optical error. Generally, the precision of a single CCD measurement is roughly 10%.

(2) System error

The system error represents the velocity error caused by mean velocity replacing instantaneous velocity. Namely, we replace Euler velocity with Lagrange mean velocity; the actual measurement is:

$$\overline{\boldsymbol{V}} = \frac{1}{\Delta T} \int_{t_0 - \frac{\Delta T}{2}}^{t_0 + \frac{\Delta T}{2}} \boldsymbol{V}(x, y, z, t) dt. \tag{6}$$

The vector $\Delta \boldsymbol{X}$ resolves into $(\Delta x, \Delta y, \Delta z)$, and accordingly, $\boldsymbol{V}$ resolves into (u, v, w).

$$u = \frac{\Delta x}{\Delta T}, \quad v = \frac{\Delta y}{\Delta T}, \quad w = \frac{\Delta z}{\Delta T} \quad (\text{supposing } S = 1).$$

For adopting a slice light beam,

$$\Delta y = 0, \boldsymbol{V} = u\boldsymbol{i} + w\boldsymbol{k}\ .$$

Suppose that the coordinates of the measured particle are (x_0, y_0, z_0, t_0), so

$$\begin{aligned} \boldsymbol{V}(x, y, z, t) = {} & \boldsymbol{V}(x_0, y_0, z_0, t_0) \\ & + \left(\Delta x \frac{\partial}{\partial x} + \Delta z \frac{\partial}{\partial z} + \Delta t \frac{\partial}{\partial t} \right) \boldsymbol{V}_0 \\ & + \frac{1}{2} \left(\Delta x \frac{\partial}{\partial x} + \Delta z \frac{\partial}{\partial z} + \Delta t \frac{\partial}{\partial t} \right)^2 \boldsymbol{V}_0. \end{aligned} \tag{7}$$

With $\Delta x = u\Delta T, \Delta z = w\Delta T$, Eq. (7) is transformed to:

$$\begin{aligned} \boldsymbol{V}(x, y, z, t) = {} & \boldsymbol{V}(x_0, y_0, z_0, t_0) \\ & + \left(u \frac{\partial}{\partial x} + w \frac{\partial}{\partial z} + \frac{\partial}{\partial t} \right) \boldsymbol{V}_0 \Delta t \\ & + \frac{1}{2} \left(u \frac{\partial}{\partial x} + w \frac{\partial}{\partial z} + \frac{\partial}{\partial t} \right)^2 \boldsymbol{V}_0 \Delta t^2, \end{aligned} \tag{8}$$

where $\Delta t = t - t_0$, therefore

$$\begin{aligned} \boldsymbol{V}(x, y, z, t) = {} & \boldsymbol{V}(x_0, y_0, z_0, t_0) \\ & - \frac{1}{24} \left(u^2 \frac{\partial^2}{\partial x^2} + w^2 \frac{\partial^2}{\partial z^2} + \frac{\partial^2}{\partial t^2} \right) \boldsymbol{V}_0 \Delta T^2. \end{aligned} \tag{9}$$

Since ΔT is very small (0.08) in this paper, the proportion of the second term in Eq. (9) is very small, and thus it can be neglected.

(3) The influence of aluminum powder gravity to velocity measurement

The aluminum powder immersed in water will suffer from gravitation, buoyancy, and drag. When aluminum powder descends, three kinds of force balance quickly:

$$\frac{1}{6} \pi D^3 g \left(\rho_{\mathrm{Al}} - \rho_{\mathrm{H_2O}} \right) = 3\pi \eta D w, \tag{10}$$

where D is the diameter of the aluminum powder, ρ_{Al} and $\rho_{\mathrm{H_2O}}$ are aluminum density and water density respectively, and η is coefficient of viscosity. From Eq. (10) and from experimental measurement, we obtain that the descending velocity is less than 0.001 m s^{-1}. As long as the diameter of the aluminum powder is fine enough, the influence of the gravity on the measurement is minor.

7. Conclusions and discussion

This paper makes use of a tank to simulate the CBL and analyze the velocity field with the PIV technique. The modeled CBL shows the development process and structure characteristic similar to those in the real atmospheric convection boundary layer. The major conclusions are as follows:

(1) The velocity distribution in the mixed layer has the characteristic of thermals in the CBL; ascending velocity is big while the descending velocity is small. The scale of the thermals increases with the rising of the mixed layer, which enlarges in the development course of the CBL.

(2) The velocity distribution in the top zone of the mixed layer exhibits well the characteristics of the entrainment layer. The ascending area becomes a descending area, and horizontal motion is evident, which embody the continuity characteristics of fluid motion.

(3) The vertical distribution of the velocity characteristic value is reasonable, which agrees with field observation and similar convection tank experiment results.

(4) The error analysis indicates good following nature of tracers. The velocity measurement truly shows the motion characteristic of the fluid, thus the reliability of the results can be proved.

Evidence is presented in support of the conclusion that the laboratory model can be a useful method in a detailed study of turbulence, and the PIV technique is feasible, though some faults in the measurement conditions still exist, such as the CCD field of view being too narrow, but the measurement scheme and analysis method are reasonably reliable. We will improve the

experimental conditions in the future and go deep into careful research of the velocity field.

Acknowledgments. This paper was supported by the National Natural Science Foundation of China under Grant Nos. 40075004 and 40105002.

REFERENCES

Coupland, J. M., C. J. D. Pickering, and N. A. Halliwell, 1987: Particle image velocimetry-theory of directional ambiguity removal using holographic image separation. *Appl. Opt.*, **26**(9), 1576–1578.

Deardorff, J. W., 1969: Numerical study of heat transport by internal gravity waves above a growing unstable layer. *Phys. Fluids*, Suppl, II, **12**, 184–194.

Host-Madsen, A., and D. R., McCluskey, 1994: On the accuracy and reliability of PIV measurements. Proceedings of the 7th international symposium on application of laser techniques to fluid mechanics, Lisboa, Portugal, July 11–14, 1994, Springer Verlag, 214–226.

Jiang Weimei, Wu Xiaoming, and Zhou Chaofu, 1991: *Physical Simulation for Atmospheric Environment*. Nanjing University Press, Nanjing. 428pp. (in Chinese)

Kaimal, J. C., J. C. Wyngaard, and D. A. Haugen, 1976: Turbulence structure in the convective boundary layer. *J. Atmos. Sci.*, **33**, 2125–2169.

Lauterborn W., and A. Vogel, 1984: Modern optical techniques in fluid mechanics. *Ann. Rev. Fluid. Mech.*, **16**, 2–23.

Lu, J., and S. P. Arya, 1997a: A laboratory study of the urban heat island in a calm and stably stratified environment. Part I: Temperature Field. *J. Appl. Meteor.*, **36**(10), 1377–1391.

Lu, J., S. P. Arya, 1997b: A laboratory study of the urban heat island in a calm and stably stratified environment. Part II: Velocity Field. *J. Appl. Meteor.*, **36**(10), 1392–1402.

Miao Shiguang, Jiang Weimei, Li Xin, and Liu Heng, 2000, Improvement of the large eddy simulation model and study on the entrainment rate. *Chinese Journal of Atmospheric Sciences*, **25**(1), 25–37. (in Chinese)

Stull, R. B., (translated by Yang Changxin), 1991: *An Introduction to Boundary Layer Meteorology*. China Meteorological Press, Beijing, China, 478–480. (in Chinese)

Sun Jianning, Jiang Weimei, Zeng Zongyong, Yuan Renming, and Yao Keya, 2000: A laboratory simulation of CBL in a water convection tank. *Journal of Nanjing University (Natural Sciences)*, **36**(6), 786–790. (in Chinese)

Willert, C. E., and M. Gharib, 1991: Digital particle image velocimetry. *Experiments in Fluids*, **10**, 181–193.

Willis, G. E., and J. W. Deardorff, 1974: A laboratory model of the unstable planetary boundary layer. *J. Atmos. Sci.*, **31**, 1297–1307.

Yuan Renmin, 2000: Experimental study on CBL in indoor laboratory. Ph. D dissertation, Anhui Institute of Optics and Mechanics, Chinese Academy of Sciences, Hefei, 117pp. (in Chinese)

实验速度场测量技术及对流边界层特征研究

李萍阳　蒋维楣　孙鉴泞　袁仁民

摘　要

在对流槽中对对流边界层（CBL）温度场实验研究的基础上，进一步尝试通过实验技术测量速度场并分析研究CBL中的速度场特征。在应用PIV测量技术时选用铝粉作示踪粒子。实验证明了在混合层中速度分布明显具有对流边界层热泡特性；混合层顶部的速度分布很好地反应出夹卷层的结构特征；湍流速度特征量的垂直分布合理，与野外实测结果和类似的对流槽实验结果接近；误差分析表明示踪粒子的跟随性良好，粒子速度的测量结果能真实地反应流体的运动特征，从而得证了分析结果的可靠性。

关键词:对流边界层, 水槽实验, PIV技术, 速度场特征分析